MESOMECHANICAL ANALYSIS OF CONCRETE UNDER LOADING THAT GENERATES ROTATION OF CRACKING

L. PUIGGRÓS[*], C.M. LÓPEZ[*] M. RODRÍGUEZ[*] AND I. CAROL[*]

[*] Department of Geotechnical Engineering and Geo-Sciences
Universidad Politécnica de Cataluña
Jordi Girona 1, Edif. D2, E-08034 Barcelona, Spain
e-mail: luispuiggros@gmail.com, carlos.maria.lopez@upc.edu,
mariana.rodriguez@upc.edu,ignacio.carol@upc.edu

Key words: Fracture in concrete, Mesomechanical analysis, Interface elements.

Abstract. Willam´s test has been often used to compare constitutive models which take into account induced anisotropy due to damage and cracking. This numerical test emulates the continuous rotation of the principal stress and deformation directions, with secondary cracks forming at inclined directions while original primary cracks aligned with the axes tend to close. However, a realistic verification of this type of behavior is limited by the absence of experimental results in the literature of concrete and other quasi brittle materials, which can be explained in part due to the complexity of practical difficulties in this kind of lab test. As a first way to cover this gap, this paper presents numerical results of a concrete meso-structural model under imposed deformations at the boundary similar to the Willam's test. The results presented include the evolution of average stress components over the sample, cracking state, etc. Generally speaking, the results obtained agree well with the predictions of advanced continuum-type anisotropic models, although some specific aspects are pointed out that would deserve further detailed study and discussion.

1 INTRODUCTION

One of the advantages of numerical models is that they allow us to replace or supplement costly experimental tests. However, numerical models need validation, and for some complex aspects on the behavior of concrete and other quasi-brittle materials, at present there are not experimental tests available to compare with. This is the case in general for loading cases implying rotation of principal stresses inside the material, which are precisely crucial to fit some macroscopic models used in structural analysis.

In particular, Willam *et. al.* [1] proposes a theoretical test in which the imposed loading process leads to a continuous rotation of the strain and stress principal direction. This test has been extensively used to check and compare different cracking and damage models [2-5], and it consists of a 2D square specimen in plane stress condition subject to the following two-step loading history under displacement control on all boundaries (Fig. 1):

- During the first step, uniaxial tension is applied along x-axis until $\sigma_I = \sigma_N = \sigma_y = f'_t$, that is, until tensile cracking just initiates. The lateral strain is given by the Poisson's coefficient during this step, i.e. in the ratio: $\Delta\varepsilon_{xx} : \Delta\varepsilon_{yy} : \Delta\varepsilon_{xy} = 1 : -v : 0$.

- In the second step, biaxial tension combined with shear deformation $\gamma_{xy} > 0$ is applied. The applied relation is: $\Delta\varepsilon_{xx} : \Delta\varepsilon_{yy} : \Delta\varepsilon_{xy} = 1 : 1.5 : 1$, or which is the same: $\Delta\varepsilon_{xx} : \Delta\varepsilon_{yy} : \Delta\gamma_{xy} = 0.5 : 0.75 : 1$.

Figure 1 schematically shows the two loading steps. In the first step cracking shows a vertical orientation, perpendicular to the tension load direction. In the second step, the combined tension and share load generate a rotation of the principal stresses which are reflected by secondary cracking forming an angle with the original cracking orientation.
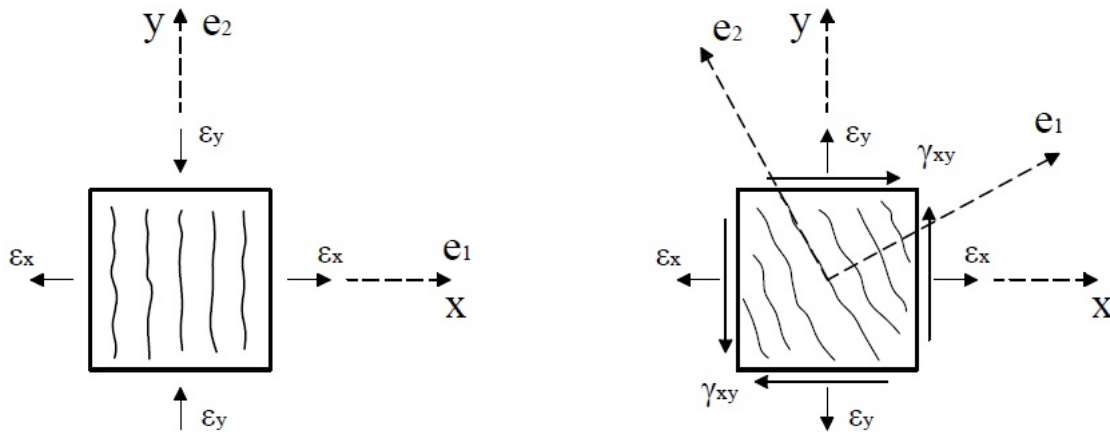

Figure 1: First step (left) and second step (right) of the theoretical test proposed in [1].

This paper describes numerical results for the Willam's test, obtained with a mesostructural model representing concrete at the level of larger aggregate particles floating on a mortar matrix. This model, developed previously by the authors is briefly described in the following paragraphs.

2 MESOMECHANICAL MODEL

The meso-mechanical model used for the simulation has been developed in the group of Mechanics of Materials UPC, during the last 15 years, firstly in 2D and later extended to 3D. In this model, the largest aggregate particles are represented explicitly, and are surrounded by a homogeneous matrix representing the average behavior of mortar plus the smaller aggregates. In order to capture the main potential crack trajectories, zero-thickness interface elements are inserted a priori of the analysis, along all the aggregate-mortar and some of the mortar-mortar mesh lines. These interface elements are equipped with a nonlinear constitutive law based on elasto-plasticity and concepts of fracture mechanics, which is formulated in terms of normal and shear components of the stress on the interface plane and the corresponding relative displacement variables. The initial loading (failure) surface $F = 0$ is given as three-parameters hyperbola (tensile strength χ, asymptotic cohesion c and asymptotic friction angle $\tan\phi$). The evolution of F (hardening-softening laws), is based on the internal variable W_{cr} (work spent in fracture processes), with the two material parameters G_F^I and G_F^{IIa} that represent the classical fracture energy in Mode I, plus a second fracture energy for an "asymptotic" Mode IIa under shear and high confinement. A more detailed description of this

elasto-plastic constitutive law can be found in the literature [6,7]. Results of the meso-mechanical model for normal concrete specimens subject to a variety of loading cases in 2D and 3D, such a uniaxial and biaxial tension and compression, brazilian test, etc. can be found in [8-10], later extended to other more complex phenomenon such a drying shrinkage, sulfate attack, high temperature [11-13].

3 NUMERICAL RESULTS

Figure 2 shows the FE mesh used for the numerical simulation of the Willam's test. In the center zone of mesh an internal framework of zero-thickness interface elements was introduced. These elements are equipped with a linear elastic behavior with high normal and tangential stiffness values, so that their presence does not alter the numerical solution. In this way, a quantification of the normal and shear stresses transmitted across this framework located far from the boundary perimeter, is obtained without interference with the original numerical solution.
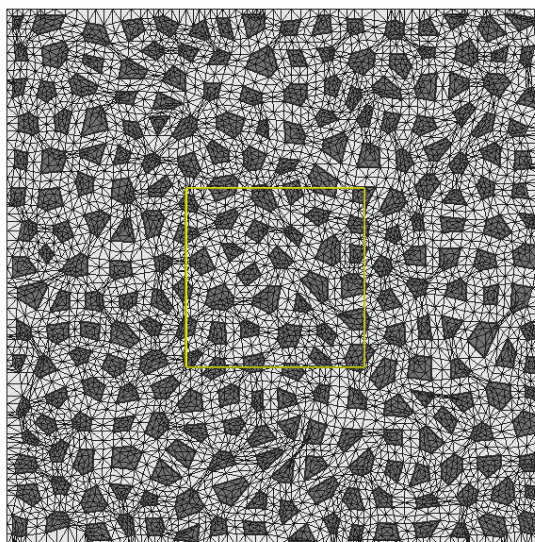

Figure 2: Finite element mesh for concrete used for numerical simulation.

The specimen dimensions used for the calculations are 30 by 30 cm, with aggregate size approximately equal to 14.5 mm and volume fraction 28%. The total no. of elements in the mesh are 12870 continuum elements and 8685 interface elements, and total no. of nodes is 19063. The material parameters are: E = 70000 MPa (aggregates), E = 25000 MPa (mortar) y υ = 0.2 (both); for the interface elements: $K_N = K_T$ = 500000 MPa/mm, $tan\phi_0$ = 0.70, χ_0 =2 MPa, c_0 = 7 MPa, G^F_I = 0.12 N·mm, G^F_{II} = 10· G^F_I, σ_{dil} = 40 MPa, α_{dil} = 2, $tan\phi_r$ = 0.4, α_ϕ = -2 and others parameters equal to zero; for mortar-mortar interface elements the same parameter were used except to χ_0 =4 MPa, c_0 = 14 MPa, G^F_I = 0.24 N·mm. The interface elements of the internal framework have an elastic behavior with high values of K_N and K_T. The tests were performed in plane stress conditions.

Figure 3, 4 and 5 show the numerical result obtained by considering the external edge as the "control framework", that is the framework along which average normal and shear

stresses are evaluated. Figure 3 shows the evolution of normal stresses on the horizontal (top) and vertical (right) faces of specimen, and the average tangential stresses obtained on the upper and right edges, all obtained as the sum of reactions divided by side dimensions, as functions of the "x" direction strain, ε_{xx}. In Fig. 3, five points have been indicated to identify the stage in the overall loading sequence: point 1 which corresponds to end of the first loading step (uniaxial tension) when maximum tension load in "x" direction is reached, and the application of the rotating strain of step two starts. We can observe that stress σ_{xx} first increases with a practically constant slope, followed by a peak (point 1) and then softening behavior. The other four points (2, 3, 4 and 5) marked on Fig. 3 correspond to different moments of the second load step. Stress σ_{yy} on its side, also shows an elastic-peak-softening curve although a little delayed with respect to σ_{xx}. Point two corresponds to an intermediate state between the peaks of σ_{xx} and σ_{yy}, whereas point three corresponds approximately to the peak of σ_{yy}. Point four has been chosen approximately close to the value 0.0003 of the xx-strain, and finally point 5 corresponds to the end of the numerical analysis. At the beginning of the second load step, normal stress σ_{xx} starts to decrease while σ_{yy} and shear stresses τ_{xy} and τ_{yx} start to increase. Note that the peak of σ_{yy} is lower than that of σ_{xx}, since the direction of secondary cracking is not perpendicular to the original cracking, and so there is an influence of the originally degraded material behavior. On the other hand, softening of the σ_{yy} curve turns out is less pronounced that of σ_{xx}. Similar evolution are observed for tangential stresses, which increase until a maximum value (lower than that for the normal stresses) followed by a softening branch. Note that there are two values of shear stress as that average is evaluated independently for the upper and right boundaries of the heterogeneous specimen.
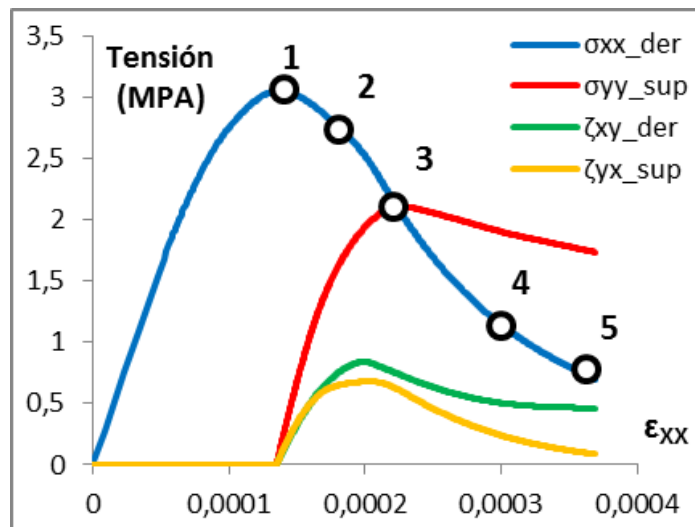

Figure 3: Evolution of normal and shear stress .vs. x direction strain, for the external framework (upper and right edge as a control frame).

Figure 4 depicts the evolution of normal stresses in the *x* and *y* directions again, together with the principal stress values σ_1 and σ_2.

Figure 5 represents the evolution of the angle of the major principal stress with respect to the *x*-axis, θ, as well as the similar angle of the major principal strain direction φ. Both angles remain equal to zero for the first load step, and then start to increase from the beginning of the

second load step. The rotations of both stress and strain directions are clearly faster at the beginning and then progressively slower. The loading boundary conditions of the test are applied through an imposed deformation and therefore the evolution of the strain direction φ is actually a prescribed magnitude with final value tending asymptotically to 52.02º [5]. The evolution of the stress direction θ, in contrast, is an outcome of the analysis. It has to be noted that the rotation of the (resulting) stress turns out significantly more pronounced than that of the (prescribed) strain, with a final value tends asymptotically to 70º. This 'over-rotation' of the resulting stress (as compared to the prescribed strain) has been reported in the literature of continuum-type models, and it is remarkable and quite reassuring that it is also observed in this meso-mechanical analysis.
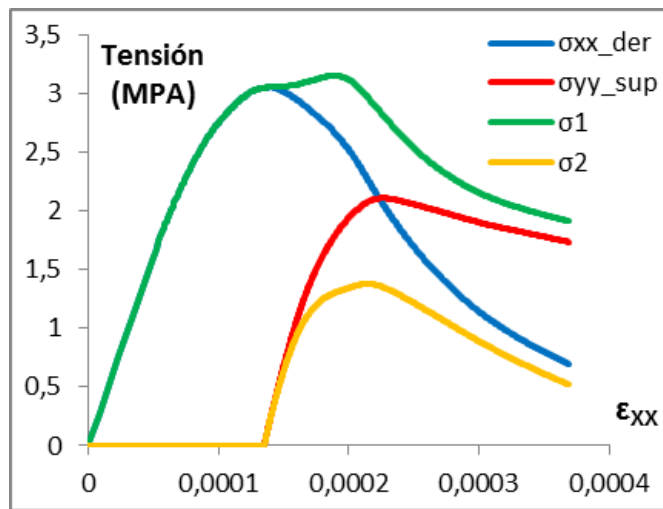

Figure 4: Evolution of average normal and principal stresses .vs. x-direction strain, for the external framework (computed on upper and right edges).
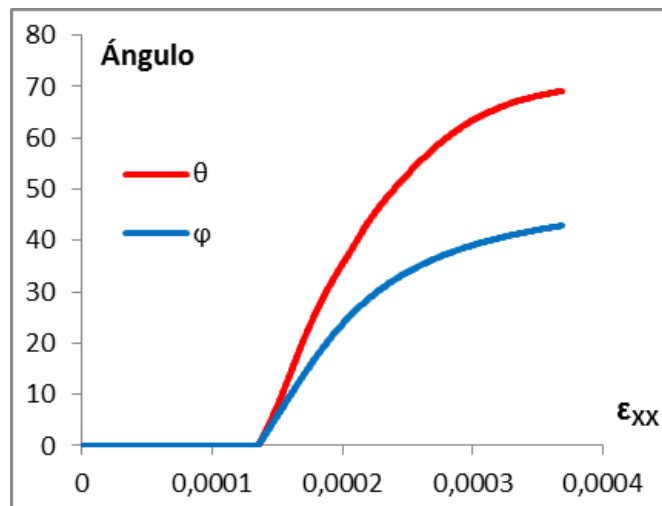

Figure 5: Variation of the angle of major principal stress direction (θ) and of major principal strain (φ) .vs. x-direction strain, for the external framework (upper and right edges).

The average stresses computed along the internal control frame, are represented in figures 6 to 9. These results were obtained from the normal and shear stress distributions obtained along the elastic interface elements introduced along the internal frame perimeter (Fig. 1). Same as before, in all the figures, the x-axis represents the always-increasing prescribed strain on the outer boundary. Figure 6 shows evolution of the average normal and shear stresses on the lower and left sides of the internal frame. The evolution of the stresses is similar to that obtained for the external frame, although the maximum values reached seem about 20-30% lower.
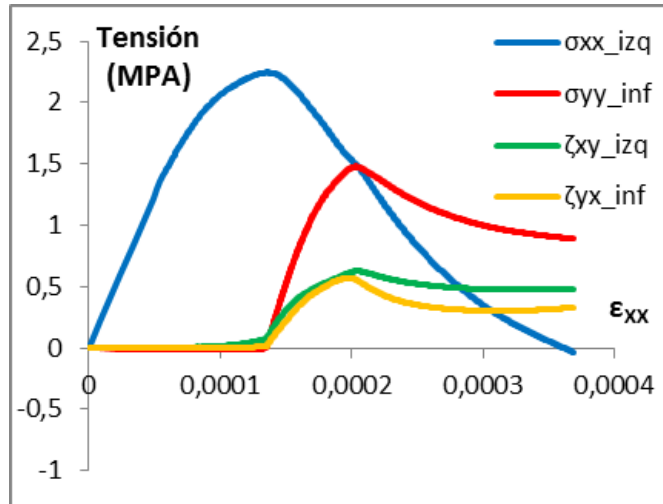

Figure 6 : Evolution of normal and shear average stress on the left and lower sides of the internal frame, *vs x*-direction prescribed strain (horizontal axis).

Figure 7 and 8 show again the evolution of average normal stresses on the left and lower faces (Fig 7) and upper and right faces (Fig. 8) of the inner frame, but this time together with the corresponding principal values stresses σ_1 and σ_2. It can be observed that both principal stresses have a similar evolution to that obtained for the external frame. During the first load step principal stresses remain $\sigma_1 = \sigma_{xx}$ and $\sigma_2=0$, but during the second step σ_{yy} and shear stresses τ_{xy} and τ_{yx} start to take values and the principal stresses become higher and lower than the normal stresses on the internal frame faces. The results in Fig 7 and 8 do not coincide exactly due to the material heterogeneity, reason for which a new procedure is being devised to obtain a consistent average stress which overcomes this duplicity. With respect to the features of the curves, most relevant seem the second peak observed in the major principal stress curve, which matches the predictions observed also in some continuum models [5, 14], and the sign inversion of the normal stress on some of the faces, which upon the prescribed strain action change from tension to compression due to the dilatancy associated to the shear sliding of the diagonal (secondary) cracks.

The evolution of the angle of the major principal stress with respect to the *x*-axis, θ, for upper-right and lower-left sides of internal frame are shown in figure 9. It can be seen that both evolution curves follow a similar trend, which it is also similar to that obtained for the external frame (figure 5).
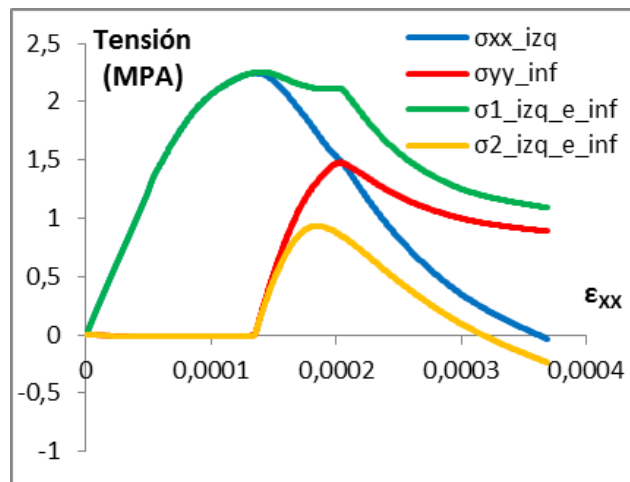
Figure 7 : Evolution of average normal and principal stress on the lower and left edges of the internal frame, *vs* the *x*-direction prescribed strain.
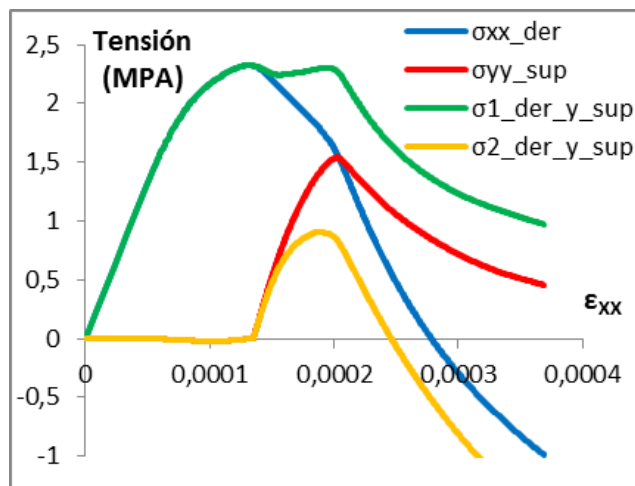

Figure 8 : Evolution of average normal and principal stress on the upper and right edges of the internal frame, *vs* the *x*-direction prescribed strain.
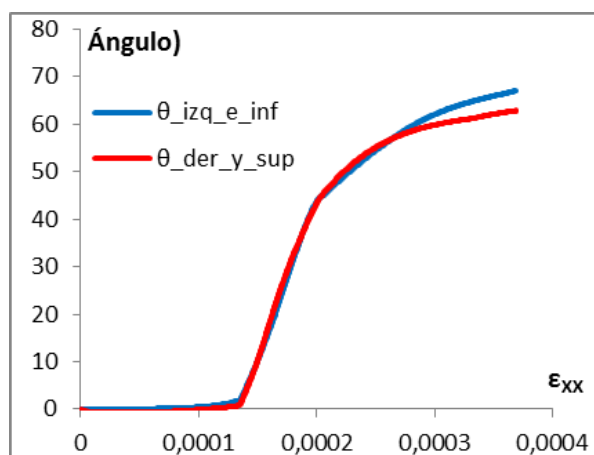

Figure 9 : Evolution of the angle of the major principal stress direction, as computed on the internal frame, as a function of the *x*-direction component of the externally prescribed strain.

1049

Figure 10 shows the evolution of cracking state, for the five points indicated in figure 3. Cracks are represented with thickness proportional to the value W_{cr}/G_F^I (energy spent in the fracture process, normalized w.r.t. the fracture energy parameter in mode I). Blue color indicates elastic unloading while red color indicates an active (opening) state for the interface.

Figure 10a left corresponds to the end of first load step (uniaxial tension) with cracking mainly in the vertical direction. Fig. 10b, c d and e, correspond to points 2, 3, 4 and 5 of figure 3, showing that opening cracks (in red) are getting re-oriented according to the rotating prescribed strain, while original cracks progressively unload (in blue). Also, with loading cracks tend to localize, with a major diagonal crack with a bridge in the middle dominating the scene and reaching the specimen boundaries (external frame). The final deformation state at the end of the test is shown in figure 10f.
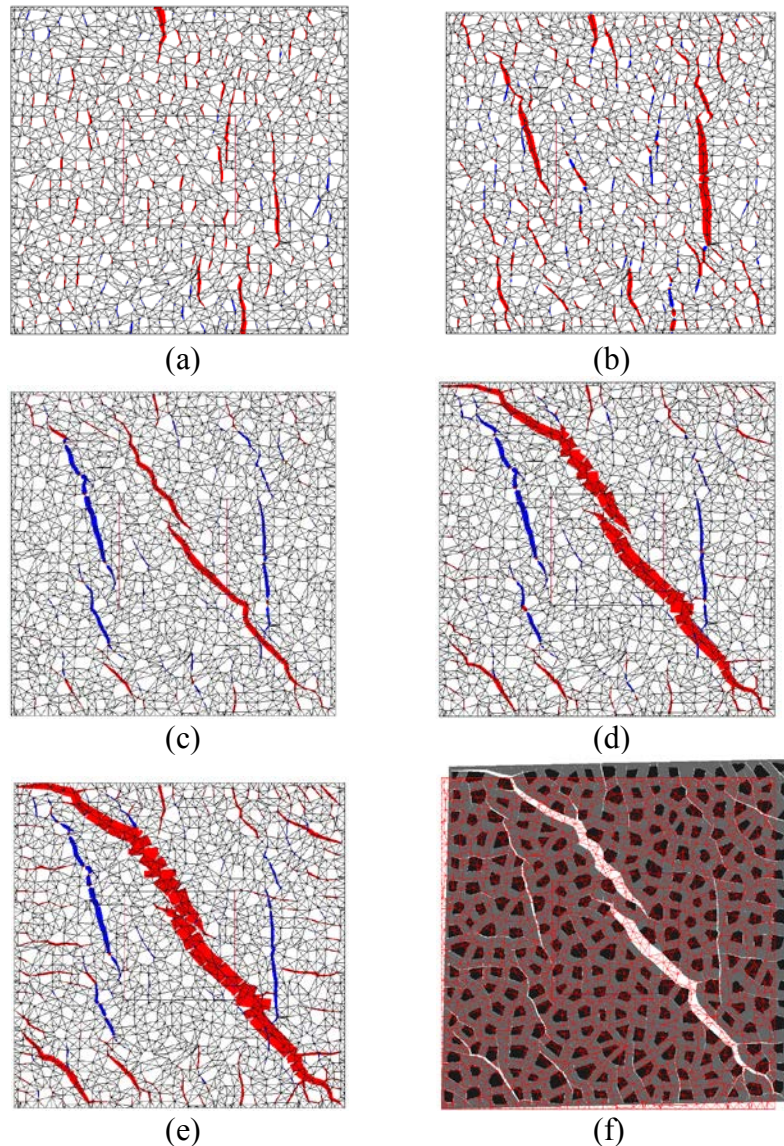

(a)

(b)

(c)

(d)

(e)

(f)

Figure 10: Evolution of cracking in terms of the dissipated energy during the fracture process (scale factor 1), for point 1 (a), 2 (b), 3 (c), 4(d) and 5(e) marked in figure 3 ((a), (b) scale factor 3 and (c), (d), (e) scale factor 1), and final deformation state (f). Red is for opening cracks, and blue is for closed cracks.

4   CONCLUDING REMARKS

Numerical results of the Willam's test at the meso-level have been obtained for a concrete specimen, using a numerical model previously developed in the group and extensively tested and verified. This test, which involves rotation of principal stress and has been often used as a benchmark test for continuum-type anisotropic models, has not been conducted experimentally so far due to the complexities lo load application, etc., and therefore the meso-level solution has an additional value as reference solution for continuum-level model testing. The results show generally the expected trends in terms of stress components evolution and rotation of principal stress directions, confirming features such as second peaks of principal stresses, and stress over-rotation with respect to prescribed strain. The results also show new intriguing aspects that open lines for future research, such as the different values of stresses in various sides of the control frames, and the influence of some aspects of the constitutive interface model on the results obtained, particularly the unloading criterion.

ACKNOWLEDGMENTS

REFERENCES

[1] Willam, K., Pramono, E., Sture, S. Fundamental issues of smeared crack models. *International conference on fracture concrete and rock*, Houston, Texas, June 17-19, 1987.

[2] Rots, J. G. Computational modelling of concrete fracture. *PhD Thesis*, University of Technology, Delft 1988.

[3] Kroplin, B., Weihe, S. Constitutive and geometrical aspects of fracture-induced anisotropy. In Owen, D.R., Oñate. E., Hinton, E. (Eds). *Computational Plasticity (COMPLAS V)*, vol.1, Pineridge, Barcelona, pp.255-279 (1997).

[4] Meschke, G., Macht, J., Lackner, R. A damage-plasticity model for concrete accounting for fracture-induced anisotropy. In Mang, H., Bicanic, N., de Borst, R. (Eds). *Computational Modelling of Concrete Structures*, Balkema, Badgastein, (Austria), pp. 3-12 (1998).

[5] Carol, I., Rizzi, E., Willam, K. On the formulation of anisotropic elastic degradation. II. Generalized pseudo-Rankine model for tensile damage. *International Journal of Solids and Structures*, vol.38, pp.519-546 (2001).

[6] Carol, I., Prat, P. C., López, C. M. A normal/shear cracking model. Application to discrete crack analysis. *J. Engng. Mech. ASCE*, 123, pp. 765−773 (1997).

[7] Carol, I., López, C.M., Roa, O. Micromechanical analysis of quasi-brittle materials using fracture-based interface elements. *Int. J. Num. Methods in Engineering*, 52(1-2), 193-215 (2001).

[8] López C.M., Carol I., Aguado A. Meso-structural study of concrete fracture using interface element. I: numerical model and tensile behaviour. *Materials and Structures*, Vol. 41, Nº 3, pag. 583-599 (2008).

[9] López C.M., Carol I., Aguado A. Meso-structural study of concrete fracture using interface element II: compression, biaxial and Brazilian test. *Materials and Structures*, Vol. 41, Nº 3, pag. 601-620 (2008).

[10] Caballero, A., López, C.M., Carol, I. 3D meso-structural analysis of concrete specimens under uniaxial tension. *Comput. Methods Appl. Mech. Engrg.*, 195, 7182-7195 (2006).

[11] Idiart, A.E., López, C.M and Carol, I. Modeling of drying shrinkage of concrete specimens at the meso-level. *Mat. and Structures*, 44:415-435 (2011).

[12] Idiart, A.E., López, C.M and Carol, I. Chemo-mechanical analysis of concrete cracking and degradation due to external sulfate attack: a meso-scale model. *Cement and Concrete Composites*, vol 33, pp. 411-423 (2011).

[13] Pérez, A., Rodríguez, M., López, CM., Carol, I. 3D-Mesomechanical Analysis of Cracking and Spalling of Concrete subjected to High Temperatures. *XII International Conference on Computational Plasticity. Fundamentals and Applications COMPLAS XII*. E. Oñate, D.R.J. Owen, D. Peric and B. Suárez (Eds). pp. 1015-1025 (2013).

[14] Carol, I. and Prat, P.C., 1995. A multicrack model based on the theory of multisurface plasticity and two fracture energies. In Owen, D.R.J., Oˇnate, E., and Hinton, E., editors, Computational Plasticity (COMPLAS IV), Vol. 2, pp. 1583–1594, Barcelona, 1995. Pineridge Press.